Weierstraß-Institut
für Angewandte Analysis und Stochastik
Leibniz-Institut im Forschungsverbund Berlin e. V.

Preprint ISSN 2198-5855

Supercontinuum generation by multiple scatterings at a group velocity horizon

Ayhan Demircan[1], Shalva Amiranashvili[2], Carsten Brée[2],

Uwe Morgner[1], Günter Steinmeyer[3]

submitted: Januar 09, 2014

[1] Leibniz Universität Hannover
Welfengarten 1
30167 Hannover
Germany
E-Mail: demircan@iqo.uni-hannover.de
morgner@iqo.uni-hannover.de

[2] Weierstraß-Institut
Mohrenstraße 39
10117 Berlin
Germany
E-Mail: shalva@wias-berlin.de
bree@wias-berlin.de

[3] Max-Born-Institute
Max-Born-Str. 2a
12489 Berlin
Germany
E-Mail: steinmey@mbi-berlin.de

No. 1918

Berlin 2014

2010 *Physics and Astronomy Classification Scheme.* 42.65.Re, 42.65.Ky, 42.65.Tg, 42.81.Dp.

Key words and phrases. Supercontinuum generation, Ultrashort pulses, Optical event horizons, Nonlinear Schrödinger equation, Hamiltonian methods, Pseudo-spectral scheme.

Sh.A. gratefully acknowledges support by the DFG Research Center MATHEON (project D 14), and A.D. by the DFG. We acknowledge support by Open Access Publishing Fund of Leibniz Universität Hannover.

Edited by
Weierstraß-Institut für Angewandte Analysis und Stochastik (WIAS)
Leibniz-Institut im Forschungsverbund Berlin e. V.
Mohrenstraße 39
10117 Berlin
Germany

Fax: +49 30 20372-303
E-Mail: preprint@wias-berlin.de
World Wide Web: http://www.wias-berlin.de/

Abstract

A new scheme for supercontinuum generation covering more than one octave and exhibiting extraordinary high coherence properties has recently been proposed in Phys. Rev. Lett. **110**, 233901 (2013). The scheme is based on two-pulse collision at a group velocity horizon between a dispersive wave and a soliton. Here we demonstrate that the same scheme can be exploited for the generation of supercontinua encompassing the entire transparency region of fused silica, ranging from 300 to 2300nm. At this bandwidth extension, the Raman effect becomes detrimental, yet may be compensated by using a cascaded collision process. Consequently, the high degree of coherence does not degrade even in this extreme scenario.

1 Introduction

White-light supercontinuum (SC) generation [2] is one of the most intriguing phenomena in nonlinear fiber optics and has revolutionized the field of frequency metrology [3]. Moreover, this process has led to a number of technological advances in various fields, including but not limited to spectroscopy, optical communications, and medical imaging [4, 5, 6]. Depending on the fiber and input pulse parameters, spectral broadening during SC generation may be caused by distinctively different mechanisms. To this end, the most efficient way is given by injection of the seed pulse into the anomalous dispersion regime. Here the interplay of soliton fission (SF) [7] and the generation of phase-matched radiation in the normal dispersion regime enables extremely broad spectra at relatively low input powers. This generic mechanism has already been studied extensively, and recently new insight into this phenomenon has been brought up with unexpected analogies to other fields in physics, such as the dynamics of ultracold atoms and ocean waves [8, 9]. Furthermore, it turned out that the complex transformation processes between dispersive radiation and solitons have remarkable impact on the spectrum (for a review, see [10]). Nevertheless, spectral broadening via SF comes with a severe drawback. This mechanisms makes the SC highly susceptible to noise in the input pulse. This input noise is amplified through the modulation instability (MI), which is also always inherently provided in the anomalous dispersion regime [11, 12], even if it may play a subdominant role for SC generation. For example, the resulting poor spectral coherence was identified as the reason for the observed temporal incompressibility of these extremely broad spectra [2]. Injection of the seed pulse in the normal dispersion regime leads to spectral broadening chiefly by self-phase modulation and the accompanying Raman effect. In this dispersion regime, the sensitivity to input noise is strongly reduced, and one can achieve stable spectra that are virtually free of the spectral modulations and fluctuations seen for anomalous dispersion. Therefore, a normally dispersive seed helps to avoid the complicated quantum noise seeded temporal pulse splitting, yet the

spectral broadening also appears strongly reduced in comparison to soliton fission. This seemingly unavoidable tradeoff between broadening efficiency and loss of coherence describes the fundamental dilemma of fiber-based supercontinuum generation.

In Ref. [1], a two-color scheme for SC generation has been presented that first offered a perspective towards overcoming the above mentioned dilemma. This method relies on a collision process between a fundamental soliton and a dispersive wave. The spectral broadening is provided by a combination of soliton compression in the anomalous dispersion regime and nonlinear frequency conversion in the normal dispersion regime. In contrast to other SC generation mechanisms, the output spectra exhibit high coherence and homogeneous spectral power density as the underlying generation mechanism is independent of SF and MI. These favorable properties make the spectra highly interesting for applications, e.g., the compression into a coherent single-cycle pulse, i.e., a topic that remained rather discouraging to date. It is important to note that the exploited specific resonant interaction is given by XPM between solitons and dispersive waves, which, in turn, is inherently contained in the standard SC scenario accompanying SF [13, 14]. Moreover, this enhanced XPM mechanism does not only support the SC process, but provides a possibility of its own for SC generation encompassing more than an octave from the anomalous to the normal dispersion regime between the utilized two seed wavelengths. This principle is related to an optical analog of the event horizon [15, 16, 17]. This analog relies on the ubiquitous wave blocking phenomenon known from fluid dynamics [18, 19]. In optics, exploitation of this principle has first been suggested for a fiber Bragg grating and is known as the “optical push broom effect” [20, 21]. Recently, this scenario has been revisited from a more general perspective, with two-beam collision processes [24] or collisions of an optical pulse with a moving inhomogeneity [22, 23].

For our purposes it is important that this kind of interaction between a fundamental soliton and a dispersive wave is able to induce a frequency shift not only for a weak dispersive wave but also for a strong fundamental soliton [25]. This particular possibility for influencing the center frequency of both pulses offers significantly enhanced manipulation of optical pulses [26]. To this end, however, appropriate material parameters have to be chosen. The induced center frequency shift then results in adiabatic soliton reshaping, i.e., effectively enables control of peak power and pulse width of the soliton. Qualitatively similar reshaping behavior results from the Raman-induced soliton self-frequency shift [27] or from ionization [28], with the former causing a red-shift and the latter a blue-shift. In our case, however, the frequency shift is induced by the dispersive wave and may be used to shift the center wavelength to either direction. The resulting supercontinua exhibit a high degree of coherence.

2 Propagation model in terms of the analytical signal

In this section we outline derivation of the basic propagation equation [29, 30] using the Hamiltonian framework [31]. We start with the pulse propagation in a single-mode fiber which is described by an effectively one-dimensional propagation equation for the real-valued optical field $E(z,t)$

$$\partial_z^2 E - \frac{1}{c^2}\partial_t^2(\hat{\epsilon}E + \chi^{(3)}E^3) = 0. \tag{1}$$

Here c is the speed of light, $\chi^{(3)}$ is the third-order nonlinear susceptibility. Both bulk and geometric contributions to the fiber dispersion are encoded in the linear operator $\hat{\epsilon}$, which is defined via convolution with some effective dispersion function $\epsilon_{\text{eff}}(\omega)$. For the time being the fiber is dissipation-free, the Raman effect will be accounted for later on. For the Fourier components $E_\omega(z)$ we obtain

$$\partial_z^2 E_\omega + \beta^2(\omega) E_\omega = -\frac{\omega^2 \chi^{(3)}}{c^2} (E^3)_\omega, \tag{2}$$

where $\beta^2(\omega)c^2 = \omega^2 \epsilon_{\text{eff}}(\omega)$, and $(E^3)_\omega$ denotes Fourier transform of the nonlinear terms. The key idea is to consider Eq. (2) as a system of weakly coupled nonlinear oscillators with the "frequency" $|\beta(\omega)|$ and to transform the left-hand-side of Eq. (2) to a kind of normal form, $i\partial_z \mathcal{A}_\omega + |\beta(\omega)|\mathcal{A}_\omega$, for a suitable normal variable $\mathcal{A}_\omega(z)$. Equation (2) is then treated as a Hamiltonian one

$$i\partial_z \mathcal{A}_\omega = -\frac{\delta H}{\delta \mathcal{A}_\omega^*} \quad \text{with} \quad H = \sum_\omega |\beta(\omega)| \mathcal{A}_\omega \mathcal{A}_\omega^* + H_{\text{nonlin}}(\mathcal{A}, \mathcal{A}^*), \tag{3}$$

where H_{nonlin} generates the nonlinear terms in Eq. (2). Equation (3) provides a z-propagation version of the standard time-evolution Hamiltonian equation of the form

$$i\partial_t a_{\mathbf{k}} = \frac{\delta H}{\delta a_{\mathbf{k}}^*} \quad \text{with} \quad H = \sum_{\mathbf{k}} \omega_{\mathbf{k}} |a_{\mathbf{k}}|^2 + H_{\text{nonlin}}(a, a^*) \tag{4}$$

which is usually used to quantize fields. Remarkably, representation (4) is of importance not only for the second quantization formalism but also for the classical nonlinear waves [31]. In the latter case the creation and annihilation operators are replaced by complex fields subject to nonlinear propagation equations. For the situation at hand the complex field $\mathcal{A}(z,t)$ is introduced by the relations

$$\mathcal{A}_\omega(z) = \sqrt{\frac{|\beta(\omega)|}{2\mu_0\omega^2}} \left[E_\omega(z) - \frac{i\partial_z E_\omega(z)}{|\beta(\omega)|} \right], \quad E_\omega = \sqrt{\frac{\mu_0\omega^2}{2|\beta(\omega)|}} (\mathcal{A}_\omega + \mathcal{A}_{-\omega}^*). \tag{5}$$

It is important to stress that we perform a change of variables which works in both directions as opposed by the usual envelope definition $E(z,t) = \mathrm{Re}[\Psi(z,t)e^{-i\omega_0 t}]$, where it is impossible to express $\Psi(z,t)$ in terms of $E(z,t)$ without further assumptions such as the slowly-varying envelope approximation (SVEA). Equation (1) is transformed to the form

$$i\partial_z \mathcal{A}_\omega + |\beta(\omega)|\mathcal{A}_\omega + 2 \sum_{123|\omega} T_{\omega_1\omega_2\omega_3\omega} \breve{\mathcal{A}}_{\omega_1} \breve{\mathcal{A}}_{\omega_2} \breve{\mathcal{A}}_{\omega_3} = 0, \tag{6}$$

where we use short notations

$$\breve{\mathcal{A}}_\omega = \frac{\mathcal{A}_\omega + \mathcal{A}_{-\omega}^*}{2}, \quad T_{\omega_1\omega_2\omega_3\omega_4} = \frac{(\mu_0\chi^{(3)}/c^2)|\omega_1\omega_2\omega_3\omega_4|}{\sqrt{|\beta(\omega_1)\beta(\omega_2)\beta(\omega_3)\beta(\omega_4)|}}, \quad \sum_{123|\omega} = \sum_{\substack{\omega_1,\omega_2,\omega_3 \\ \omega_1+\omega_2+\omega_3=\omega}}. \tag{7}$$

One can check that the Hamiltonian function is given by

$$H = \sum_\omega |\beta(\omega)| \mathcal{A}_\omega \mathcal{A}_\omega^* + \sum_{1234|0} T_{\omega_1\omega_2\omega_3\omega_4} \breve{\mathcal{A}}_{\omega_1} \breve{\mathcal{A}}_{\omega_2} \breve{\mathcal{A}}_{\omega_3} \breve{\mathcal{A}}_{\omega_4}. \tag{8}$$

Further simplifications are possible if the dispersion law $\beta = \beta(\omega)$ does not support the third-harmonics generation process. Neglecting then all non-resonant terms, one obtains a much more simple expression

$$H_{\text{nonlin}} = \frac{3}{8} \sum_{1\bar{2}3\bar{4}|0} T_{\omega_1\omega_2\omega_3\omega_4} \mathcal{A}_{\omega_1} \mathcal{A}^*_{\omega_2} \mathcal{A}_{\omega_3} \mathcal{A}^*_{\omega_4} \tag{9}$$

and Eq. (6) is reduced to the form

$$i\partial_z \mathcal{A}_\omega + |\beta(\omega)| \mathcal{A}_\omega + \frac{3}{4} \sum_{1\bar{2}3|\omega} T_{\omega_1\omega_2\omega_3\omega} \mathcal{A}_{\omega_1} \mathcal{A}^*_{\omega_2} \mathcal{A}_{\omega_3} = 0, \tag{10}$$

where $\sum\limits_{\substack{\omega_1,\omega_2,\omega_3 \\ \omega_1-\omega_2+\omega_3=\omega}}$ is encoded as $\sum\limits_{1\bar{2}3|\omega}$.

The above Hamilton equations provide an easy way to derive the constants of motion. For a sequence of pulses propagating with the time period T the Hamiltonian (8) can be transformed to the form

$$H = \int_{-T/2}^{T/2} \left[\frac{\epsilon_0}{2} \left(\hat{\epsilon} E + \frac{1}{2} \chi^{(3)} E^3 \right) E + \frac{1}{2\mu_0} B^2 \right] \frac{dt}{T}, \tag{11}$$

this conserved quantity is related to the averaged momentum flux. Another conserved quantity

$$\sum_\omega \omega |\mathcal{A}_\omega|^2 = \int_{-T/2}^{T/2} \frac{EB}{\mu_0} \frac{dt}{T} = \text{const} \tag{12}$$

is the-time averaged energy flux. If we change from Eq. (6) to Eq. (10), one more constant of motion appears

$$\sum_\omega |\mathcal{A}_\omega|^2 = \sum_\omega \frac{1}{|\beta(\omega)|} \left(\frac{\epsilon_0 \epsilon_{\text{eff}}(\omega) |E_\omega|^2}{2} + \frac{|B_\omega|^2}{2\mu_0} \right) = \text{const} \tag{13}$$

and can be interpreted as the classical photon flux [29]. These constants of motions can be used to estimate energy and photon transfer between the colliding pulses if the latter are separated in the frequency domain.

We are in a good position to stress that equations (6) and (10) look like the generalized nonlinear Schrödinger equations (GNSE) and can be solved in the same way, e.g., with the split-step method. However, Eq. (6) is an exact reformulation of Eq. (1), the transformation (5) is just a change of variables. Also a non-resonant dispersion law that is required to derive Eq. (10) is a weaker assumption than the SVEA. In particular, both (6) and (10) are *bidirectional* equations. The standard GNSE is unidirectional, it appears if one additionally applies an unidirectional approximation. Indeed, let us consider how the differential operator in Eq. (5) acts on a forward (backward) wave

$$\left[1 - \frac{1}{|\beta(\omega)|} i\partial_z \right] e^{\pm i\beta(\omega) z - i\omega t} = [1 \pm \operatorname{sign} \omega] e^{\pm i\beta(\omega) z - i\omega t}. \tag{14}$$

The forward (backward) waves are mapped onto the positive (negative) frequency part of $\mathcal{A}(z,t)$. If the forward waves dominate, the negative-frequency part of $\mathcal{A}(z,t)$ can be neglected. The complex field $\mathcal{A}(z,t)$ is then directly related to the analytic signal for the electric field $\mathcal{E}(z,t)$

$$\mathcal{A}_\omega = \sqrt{\frac{|\beta(\omega)|}{2\mu_0\omega^2}}\mathcal{E}_\omega, \qquad \omega > 0, \tag{15}$$

where $\mathcal{E}(z,t)$ is just a sum of the positive-frequency components of $E(z,t)$.

$$E(z,t) = \sum_\omega E_\omega(z)e^{-i\omega t} \quad \Rightarrow \quad \mathcal{E}(z,t) = 2\sum_{\omega>0} E_\omega(z)e^{-i\omega t}. \tag{16}$$

such that $E(z,t) = \mathrm{Re}[\mathcal{E}(z,t)]$. The propagation equation for the analytic signal reads

$$i\partial_z\mathcal{E}_\omega + \beta(\omega)\mathcal{E}_\omega + \frac{\omega^2\chi^{(3)}}{8c^2\beta(\omega)}\left[(\mathcal{E}+\mathcal{E}^*)^3\right]_\omega = 0. \tag{17}$$

where the latter equation applies only for $\omega > 0$ and $\mathcal{E}_{\omega<0}$ vanishes by construction. In what follows, we ignore generation of the third harmonics and simplify Eq. (17) to the form

$$i\partial_z\mathcal{E}_\omega + \beta(\omega)\mathcal{E}_\omega + \frac{3\omega^2\chi^{(3)}}{8c^2\beta(\omega)}(|\mathcal{E}|^2\mathcal{E})_\omega = 0, \quad \omega > 0. \tag{18}$$

To return to the space-time representation, it is convenient to denote convolution with $\beta(\omega)$ in the linear term by $i\hat{\beta}$, to approximate $\beta(\omega)$ in the nonlinear term by $\omega n(\omega_0)/c$ for some reference index of refraction $n(\omega_0)$, and to use a standard notation for the nonlinear refraction, $n_2 = (3/8)\chi^{(3)}/n(\omega_0)$. Equation (18) yields

$$\partial_z\mathcal{E} + \hat{\beta}\mathcal{E} + \frac{n_2}{c}\partial_t(|\mathcal{E}|^2\mathcal{E})_+ = 0. \tag{19}$$

where $(\,)_+$ denotes the positive-frequency part. The range of applicability of Eq. (19) is similar to that of the unidirectional forward Maxwell equation [7], but with the benefit of a clear separation of third-harmonic generation terms. If the Raman effect is important, Eq. (19) is replaced by

$$\partial_z\mathcal{E} + \hat{\beta}\mathcal{E} + \frac{n_2}{c}\partial_t(f_K|\mathcal{E}|^2\mathcal{E} + f_R\mathcal{E}\hat{h}|\mathcal{E}|^2)_+ = 0, \tag{20}$$

where f_K and $f_R = 1 - f_K$ describe relative contributions of the Kerr and Raman effects and $\hat{h}$ denotes a standard convolution with the Raman response function

$$\hat{h}|\mathcal{E}(z,t)|^2 = \int_0^\infty h(t')|\mathcal{E}(z,t-t')|^2dt', \quad h(t') = \frac{\tau_1^2+\tau_2^2}{\tau_1\tau_2^2}e^{-t'/\tau_2}\sin(t'/\tau_1) \tag{21}$$

where we adopted typical values $f_R = 0.82$, $\tau_1 = 12.2\,$fs and $\tau_2 = 32\,$fs for silica fibers [2].

Figure 1 depicts an exemplary group delay profile $\beta_1 = \beta'(\omega)$ and related group-velocity dispersion profile $\beta_2 = \beta''(\omega)$ for a 5 micron strand of silica in air [32]. The presence of absorptive resonances in the ultraviolet as well as vibrational resonances in the infrared generally causes a

characteristic concave group-velocity dispersion profile, which is modified by the waveguide dispersion. For the exemplary case shown here, this results in a zero-dispersion wavelength (ZDW) located at 997 nmm wavelength. For numerical solution of Eq. (20) we use either a de-aliased pseudospectral method, with the implementation of the Runge-Kutta integration scheme in the frequency domain and adaptive step-size control, or a more direct split-step Fourier approach. Accuracy of the numerical scheme is monitored by tracing the constants of motion. Considering ultrashort optical pulses with carrier frequencies of several hundreds THz, we use a maximum temporal discretization step of $\Delta t = 0.6$fs. Sufficiency of the discretization is ensured by exemplary runs that involve a considerably larger number of harmonics.

For the calculation of the coherence properties we generated a total of 512 supercontinua instances, using different quantum noise seeds. Namely, the noise seeds are numerically implemented by adding one photon with random phase per mode to each discrete frequency bin of the input signal [2].

3 Optical event horizon inducing collisions between dispersive waves and solitons

The concave group-velocity profile of solid dielectric materials always enables co-propagation of a dispersive wave (DW) and a soliton at exactly identical group velocity, see Fig. 1 for the linear optical contributions. For an exact match, nonlinear contributions to the group velocity have to be considered. In particular, the group velocity is modified in the immediate vicinity of the soliton. Launching a DW and a soliton at nearly identical group velocities may then lead to a condition that has been termed “optical group-velocity horizon”. Once the dispersive wave reaches the nonlinear index modification induced by the soliton, both pulses remain temporally locked to each other. Consequently, the effective XPM interaction length between the two pulses is significantly increased, and any walk-off effect is prevented or at least substantially delayed.

The according group velocity dispersion β_2 profile and the relative group delay $\beta_1 = 1/v_g$ profile are shown in Fig. 1, together with a selection of three exemplary frequency combinations. The fiber group index is taken from [32]. Accordingly, for the given situation, we launch two synchronized pulses with similar pulse parameters

$$\mathcal{E}(z=0,t) = \mathcal{E}_s \,\mathrm{sech}(t/t_s) e^{-i\omega_s t} + \mathcal{E}_p \,\mathrm{sech}(t/t_p) e^{-i\omega_p t}, \tag{22}$$

where $\mathcal{E}_{s,p}, t_{s,p}, \omega_{s,p}$ correspond to the initial field, the temporal width, and the center frequency, respectively. The pulses are injected at an initial time delay of $\Delta T = 450$ fs into the fiber on either side of the zero dispersion wavelength. For demonstration of the main mechanism, we first neglect the Raman effect. In principle, such pure Raman-free behavior can be realized in hollow-core fibers filled with noble gases [28].

An exemplary collision process of a DW at the leading edge of a fundamental soliton is demonstrated in Fig. 2(a,b). The DW is injected earlier into the fiber at a frequency with a slightly slower group velocity as the FS, leading to a collision process that induces a blueshift of the soliton center frequency and a redshift of the DW [Fig. 2(b)]. Both pulses are accelerated by the collision

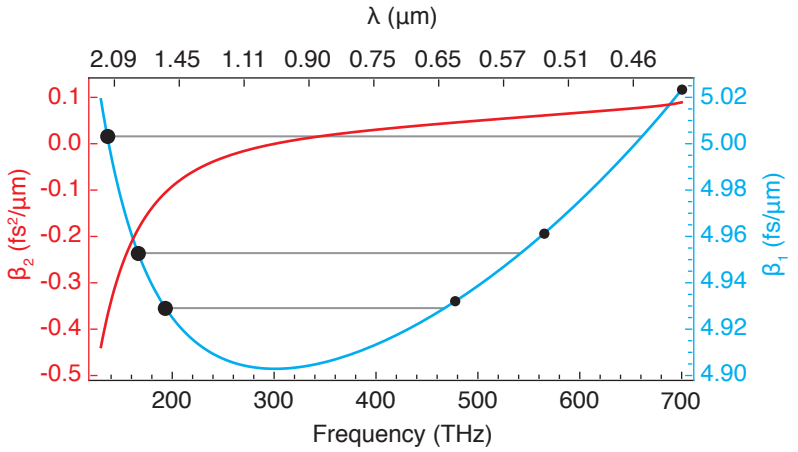

Figure 1: The group velocity dispersion β_2 and the relative group delay $\beta_1 = 1/v_g$ of a fused silica fiber, exhibiting three exemplary wavelength combinations [1550,627] nm, [1800,530] nm, and [2200,428] nm for a soliton and a probe pulse with nearly equal group velocities.

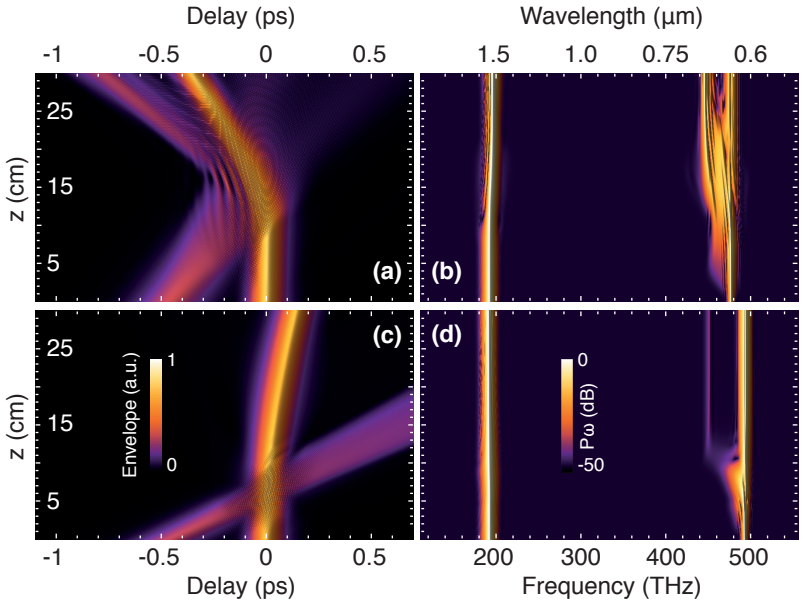

Figure 2: Time domain and spectral evolution of two pulse collision between a soliton and a dispersive wave. (a,b) Enhanced XPM for the "resonant" wavelength combination at [1550,627] nm representing the scattering process at an effective group-velocity horizon. (c,d) Typical crossing of two pulses without any repulsion for the standard XPM interaction for wavelength combination [1550,607] nm.

[26]. This process has recently also been referred to as diametrically driven self-acceleration [33]. For a comparison of this enhanced nonlinear interaction and the standard XPM, we illustrate the resulting collision process for the latter case, i.e., without the repulsion of the DW in Fig. 2(c,d). The initial wavelength of the DW is shifted away from the "resonant condition" for nearly equal group-velocities and is changed from 627 nm to 607 nm. The pulses quickly pass each other, and only a marginal change of the pulse parameters is observed. However, there exists a range of DW frequencies that establish a collision process. Given the chosen frequency of the DW, different collision scenarios can be generated while keeping all other parameters of both pulses fixed. Moving farther away from the exact resonant condition, only a part of the DW is reflected. This behavior suggests use of the DW frequency as an effective control parameter for all-optical manipulation. Other control parameters are provided by the amplitude and the width of the DW as well as by the initial time delay between both pulses. Among all these parameters, the DW amplitude represents the simplest adjustable and the most efficient control parameter.

The main idea behind the manipulation by the event horizon relies on exploitation of the induced center frequency shift of the soliton in a suitably chosen dispersion profile. Namely, the soliton has to be injected into a region with a large β_3 coefficient. The elementary collision process is completely elastic, causing a mutual shift of optical frequencies, yet without transferring photons from the normal dispersion regime into the soliton regime or vice versa. With the photon number of the soliton being conserved, the soliton blueshift is automatically accompanied by a mild energy increase. However, the blue-shifted soliton is located closer to the zero-dispersion wavelength and therefore also experiences a reduced second-order dispersion after the collision. Depending on the initial frequency of the soliton, an induced frequency shift of only a few nm may result in a considerable change of the dispersion parameter, depending on the strength of the β_3 coefficient. Considering that the energy E of a fundamental soliton relates to P_0 and β_2 via

$$E = 2\sqrt{P_0|\beta_2|/\gamma}, \tag{23}$$

the reduction of β_2 cannot be compensated by a decrease of E because E is nearly constant and may even slightly grow due to the increase of photon energy. As γ also does not vary appreciably with wavelength, Eq. (23) therefore affects a massive growth of P_0 as a result of the blue shift. Moreover, as the pulse energy is nearly conserved, this peak power growth is automatically accompanied by a decrease in pulse width. In summary, one can understand the reshaping process of the soliton as an adiabatic compression mechanism that is induced by the DW via mutual four-wave mixing processes. A reverse scenario where the DW is reflected at the trailing edge of the soliton also results in the opposite effect. In the latter case both pulses are decelerated due to their interaction. Consequently, the soliton is not compressed, which renders this situation unsuitable for SC generation.

4 SC generation by soliton collision with dispersive waves

The importance of DWs, in particular their initial generation and subsequent transformation by the solitons, has already been demonstrated in the soliton-fission dominated SC generation, where it leads to additional spectral broadening [10, 13, 34]. However, the underlying process

may also be employed for direct generation of the supercontinuum without the fission process. To this end, one has to provide a continuous repulsion of dispersive waves at the temporal location of the soliton. Background radiation with a suitable frequency for a repulsion process may be created by the dispersion of an intense and ultrashort pulse in the normal dispersion regime. The time delay between the initial DW and the soliton can then be chosen in such a way to ensure a reflection of radiation at the soliton edge over longer propagation distances, but one has to take care that the radiation amplitude is too low for inducing a soliton frequency shift at any point of the reflection process.

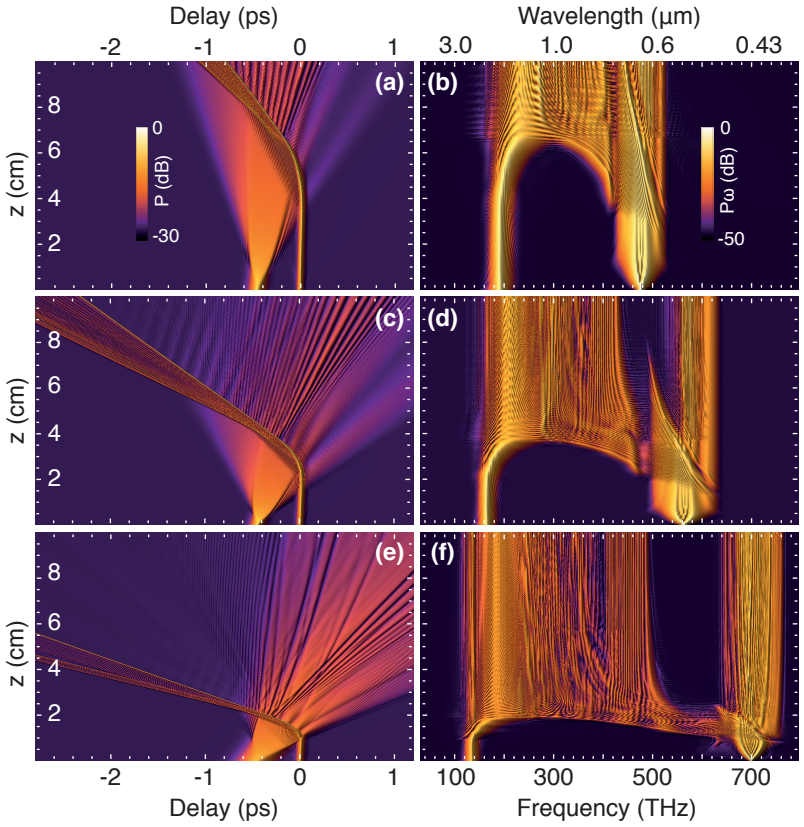

Figure 3: Supercontinuum generation by two pulse collision for the three frequency combinations marked in Fig. 1. (a,b) Supercontinuum encompassing more than an octave from the anomalous to the normal dispersion regimes for the wavelength combination [1550,627] nm. (c,d) Increased spectral bandwidth for the wavelength combination [1800,530] nm. (e,f) Supercontinuum spanning over the whole transparency region of fused silica for [2200,428] nm.

For the three frequency combinations marked in Fig. 1, time domain representations of the SC propagation dynamics are shown in Fig. 3 together with the corresponding evolution of the spectra. Detailed pulse parameters are given in Table 1. In all three cases, the width of the solitons are chosen to display an equal number of cycles at the given wavelength. Scattering of the background radiation at the edge of the fundamental soliton can be realised over long propagation distances in all three cases. In parallel, we observe that the constant acceleration of the soliton leads to a parabolic trajectory in the (t, z)-plane, which is typical for the interaction behavior at an optical event horizon. However, we have a natural limitation of the acceleration

Table 1: Pulse parameters for the soliton and dispersive wave.

	Soliton			Dispersive wave			
Figure	λ(nm)	t_0(fs)	$\frac{\beta_2}{(\text{fs}^2/\mu\text{m})}$	λ(nm)	t_0(fs)	$\frac{\beta_2}{(\text{fs}^2/\mu\text{m})}$	P_{DW}/P_{FS}
2a,b	1550	45.03	-0.105	628	100	0.0456	0.19
2c,d	1550	45.03	-0.105	608	100	0.0456	0.19
3a,b	1550	15.48	-0.105	628	40	0.0456	0.92
3c,d	1800	17.01	-0.184	530	34	0.060	1.30
3e,f	2200	20.99	-0.372	428	100	0.0894	1.00
4a,b	1800	17.01	-0.184	538	100	0.0595	1.3
4c,d	2200	20.99	-0.372	428	100	0.0894	1.0

process as the group-velocity must not exceed its maximum value given by the minimum of β_1 at the ZDW. At this point the soliton can no longer be accelerated, which terminates soliton compression. Subsequently, we finally observe a transfer of energy from the soliton into the normal dispersion regime. This final process also contributes to the SC generation.

The entire SC generation process can therefore be understood as soliton compression in the anomalous dispersion regime accompanied by the excitation of new frequencies by the reflection of the DW in the normal dispersion regime. Further contributions stem from self-phase modulation of the non-reflected part and from the above-mentioned merging of the soliton spectrum into the normal dispersion regime. Figure 3(a,b) is equivalent to the SC generation demonstrated in [1], yet for the frequency combination $[1550, 627]$nm. The attainable bandwidth of the SC is chiefly determined by the initial separation of the two frequencies. The generated spectrum exhibits a 20-dB spectral width of 1050 nm, encompassing 1.5 octaves from 570 nm to 1620 nm. In Fig. 3(c,d) we extend the separation of the frequency between the soliton and the DW from 1800nm to 520nm. To observe the same behavior, we have to increase the energy of the DW by an increase of the peak intensity or the pulse width. Figure 3(e,f) finally discusses an expansion of the wavelength separation close to the total available transparency region of the given strand fiber, i.e., 400–2400nm for fused silica. Also for this limiting example, the entire bandwidth between the two initial frequencies is continuously excited. In contrast to the SC by soliton fission, we do observe any limitation of spectral broadening. Consequently, this has to be considered a huge advantage of our scheme as it enables the generation of a SC over the whole bandwidth between the resonant absorption in the UV and the mid-infrared.

The spectral width can be adjusted by the frequency combination and the energy contents of both pulses. In general, there appears a disadvantage of the less effective spectral broadening in the normal dispersion regime [2]. However, in our case the spectral broadening depends on both pulses, and the spectral width and shape can be adjusted in different ways. It is also possible to excite only a part of the spectrum between the two pump wavelengths with high brightness in the normal dispersion regime.

Without the Raman effect, the main limitation for the obtainable spectral bandwidth is just dictated by the transparency region of the material, i.e., more than 2.5 octaves for fused silica. Depending on the material of the fiber, even broader SC may be generated, reaching into the mid-infrared if one chooses,e.g., fluoride glasses or chalcogenides.

Apart from the possibility for multi-octave SC generation, the resulting spectra exhibit extraordinary coherence properties [1]. In the normal dispersion regime, non-deterministic temporal pulse splitting is typically inherently avoided. Such behavior could translate into spectral modulation, and fluctuations are avoided. Markedly in the anomalous dispersion regime, our scheme does neither exhibit a pronounced susceptibility to noise. Usually noise is amplified in the input pulse through the modulation instability. In our case, this degeneration process is suitably avoided as the soliton pulse width becomes extremely short, which, in turn, substantially reduces the impact of the MI [12].

5 Supercontinuum generation under consideration of the Raman effect

The discussed scattering processes in the event horizon have previously reported to also appear in the presence of the Raman effect [15, 35, 8, 36, 37, 38] and the same process may therefore exploited for SC generation. For the particular frequency combination [1550,627] nm, we previously demonstrated that a SC with a similarly high degree of coherence is generated [1]. One has to justify that the properties of the DW may readily serve to pre-compensate the Raman induced soliton-self-frequency-shift (SSFS) [39]. Such pre-compensation requires only minor adjustment of input parameters. As control parameters one may use the peak power, the pulse width of the DW, or the time delay between the DW and the soliton. As only the low intensity parts of the DW are reflected, the intensity and the width of the initial DW need to be chosen such that a suitable low level background is built up by DW broadening. It should be noted that higher intensities of the DW effectively cross the trajectory of the soliton, with an accordingly smaller reflected part. Temporal broadening of the DW can easily be controlled by choosing an appropriate time delay between the soliton and the DW. At the same time, however, the intensity of the DW segments have to be high enough at any interaction point to compensate and overcome the counteracting deceleration by the self-frequency shift. This naturally implies that the group velocities of both pulses should not be chosen too close to each other, effectively limiting the range of the resonant condition for the reflection process. For further extension of the bandwidth between the two initial frequencies, compensation of the SSFS becomes increasingly difficult. Figure 4 depicts simulations that include the Raman effect for the wavelength combination [1800,530] nm and [2200,428] nm. For the spectrum that ranges from 520 nm to 1800 nm [Fig. 4(a,b)], filling the gap between the two input wavelengths with the same mechanism turns out to be possible. However, in order to do so, we need careful adjustments of several parameters. Apart from a suitable combination of the peak intensity, the width of the DW and the time delay between the DW and the soliton, we also find an adequate modulation of the DW center frequency necessary.

Further increase of the gap between the initial frequencies of DW and the soliton, now for the combination [2200,428] nm, makes it even more difficult to fill all frequencies in the gap as a compensation of the Raman effect is no longer possible for the whole necessary range [Fig. 4(c,d)]. Consequently, the interaction length between the DW and the soliton does not suffice anymore for the generation of a SC over the entire spectral range that was previously

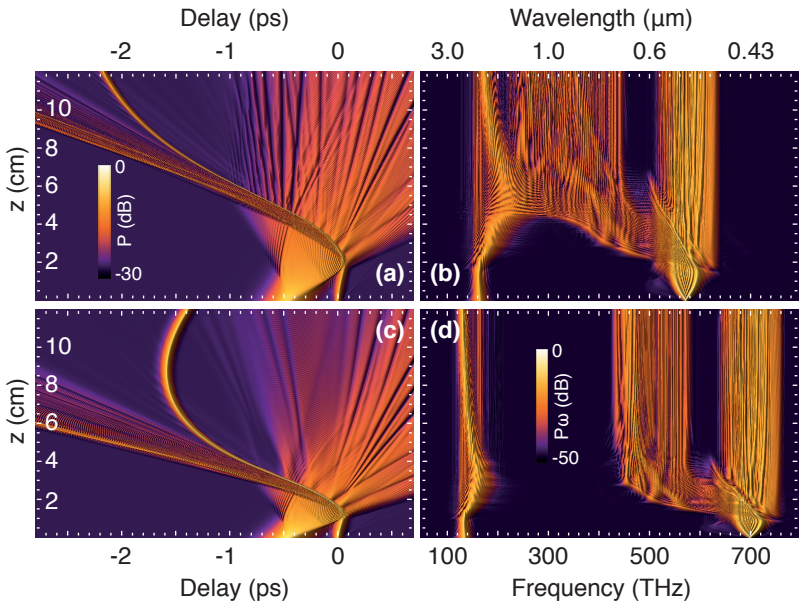

Figure 4: Evolution of the supercontinuum in the time domain and the spectral domain by two-pulse collision with the impact of the Raman effect for (a,b) the wavelength combination [1800,538] nm, and (c,d) [2200,428] nm.

discussed in the absence of the Raman effect. Including the Raman effect, the soliton trajectory is strongly influenced by the self-frequency shift. This effect pushes the soliton back towards the red, leading to adverse temporal broadening and deceleration of the soliton. Consequently, in comparison to the Raman free-case, the amplitude of the DW has always to be higher at the reflection point as the SSFS has to be compensated. For longer propagation distances, interaction of a DW with a FS may be enforced by an increase of the initial pulse width and peak intensity. However, there is another important limiting issue as the DW induced blueshift of the soliton also affects the resonance condition implied by the dispersion properties. A rapid soliton frequency sweep therefore quickly terminates effective interaction.

One possibility to overcome this obstacle is suggested in Fig. 5(a,b), where our scheme is used in a cascaded way. We inject now two DWs at different frequencies into the fiber. The wavelength of the first injected DW exhibits a centre wavelength at 470nm that is adjusted to be in resonance with soliton at a center wavelength closer to the ZDW. Despite of being injected first, this DW only interacts with the soliton after having been blue-shifted by the other primary DW. Once the effective interaction with this primary DW has come to an end, the secondary DW takes over and thereby expands the duration of effective nonlinear interaction with the soliton. In this way the whole spectrum in the transparency region can be excited as the Raman effect is compensated over longer distances. Cascaded interaction of the soliton and several DWs at different frequencies does not only enable generation of broader SCs, but also opens up a perspective for conveniently realising the necessary pulse parameters.

One of the advantages of the SC generated by two-pulse collision relates to their superior coherence properties. In the cascaded scheme, there are also no detrimental effects that could cause a degradation of the coherence properties, as MI and pulse splitting are still avoided.

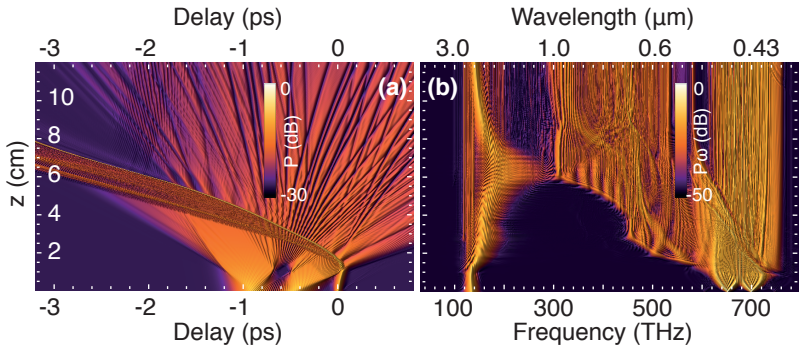

Figure 5: Multiple scattering between dispersive waves and a fundamental soliton for generation of a supercontinuum ranging over the whole transparency region. Evolution (a) in the time domain, and (b) the spectral domain. The first dispersive wave is injected at a center wavelength of 470nm. The wavelength of the dispersive wave for the primary interaction with the soliton lies at 428 nm. All other parameters are the same as for Fig. 4(c,d).

To demonstrate this, we calculate the measure of the SC phase stability by the modulus of the complex degree of first-order coherence at each wavelength [40]

$$|g_{12}(\lambda, t_1 - t_2)| = \left| \frac{\langle E_1^*(\lambda, t_1) E_2(\lambda, t_2) \rangle}{\sqrt{\langle |E_1(\lambda, t_1)|^2 \rangle \langle |E_2(\lambda, t_2)|^2 \rangle}} \right| . \tag{24}$$

The angular brackets denote an ensemble average over independently generated pairs of SC spectra $[E_1(\lambda, t), E_2(\lambda, t)]$ obtained from 512 simulations.

Figure 6(a) displays single-shot spectra for selected values of z of the fiber, using the same parameters as in Fig. 5(b). The corresponding degree of coherence [Fig. 6(b)] reflects the expected insensitivity to noise. We observe similar coherence properties for a SC that covers the whole transparency region as was previously reported for an only 1.5 octave spanning SC in Ref. [1]. The only notable degradation is found in the vicinity of the zero dispersion wavelength. Otherwise, wide spectral segments exhibit favorable coherence properties, both in the normal and anomalous dispersion regime.

6 Conclusion

We presented a novel scheme for generating a multi-octave supercontinua. This scheme is based on the strong pulse reshaping at an optical event horizon, and it consists of the combination of different mechanisms for each dispersive regime. Namely, these mechanisms are soliton compression and frequency conversion due to the reflection of dispersive waves at the effective horizon of a soliton in the anomalous and the normal dispersion regime, respectively. Our scheme bears several possibilities for tailoring properties of the SC, which enables adaption to different applications and demands. Apart from the possibility to generate different spectral coverage ranges, favorable coherence properties may be achieved, in particular also in the anomalous dispersion regime.

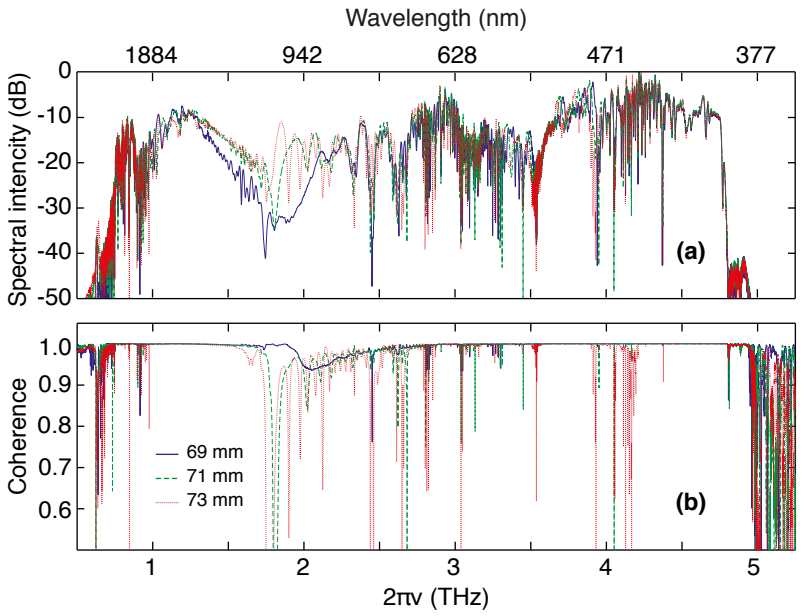

Figure 6: (a) Single shot spectra for the supercontinuum generation in Fig. 5 at different propagation distances. (b) Corresponding degree of coherence.

References

[1] A. Demircan, Sh. Amiranashvili, C. Brée and G. Steinmeyer, "Compressible octave spanning supercontinuum generation by two-pulse collisions," Phys. Rev. Lett. **110**, 233901 (2013).

[2] J. M. Dudley, G. Genty, and S. Coen, "Supercontinuum Generation in Photonic Crystal Fiber," Rev. Mod. Phys. **78,** 1135 (2006).

[3] R. Holzwarth, M. Zimmermann, Th. Udem, T.W. Hänsch, P. Russbüldt, K. Gäbel, R. Poprawe, J. C. Knight, W. J. Wadsworth, and P. St. J. Russell, "White-light frequency comb generation with a diode-pumped Cr:LiSAF laser," Opt. Lett. **26,** 1376 (2001).

[4] R. Holzwarth, T. Udem, T. W. Hänsch, J. C. Knight, W. J. Wadsworth, and P. St. J. Russell, "Optical frequency synthesizer for precision spectroscopy," Phys. Rev. Lett. **85,** 2264 (2000).

[5] K. Saitoh and M. Koshiba, "Highly nonlinear dispersion-flattened photonic crystal fibers for supercontinuum generation in a telecommunication window," Opt. Express **12**, 2027 (2004).

[6] I. Hartl, X.D. Li, C. Chudoba, R.K. Ghanta, T.H. Ko, J.G. Fujimoto, J.K. Ranka, and R.S. Windeler, "Ultrahigh-resolution optical coherence tomography using continuum generation in an air-silica microstructure optical fiber," Optics Lett. **26,** 608 (2001).

[7] A.V. Husakou and J. Herrmann,"Supercontinuum Generation of Higher-Order Solitons by Fission in Photonic Crystal Fibers," Phys. Rev. Lett. **87,** 203901 (2001).

[8] A. V. Gorbach and D. V. Skryabin, "Bouncing of a dispersive pulse on an accelerating soliton and stepwise frequency conversion in optical fibers," Opt. Express **15**, 14560 (2008).

[9] D. R. Solli, C. Ropers, P. Koonath, and B. Jalali, "Optical rogue waves", Nature **450**, 1054 (2007).

[10] D. V. Skryabin and A. V. Gorbach, "Colloquim: Looking at a soliton through the prism of optical supercontinuum," Rev. Mod. Phys. **82**, 1287 (2010).

[11] A. Demircan and U. Bandelow, "Supercontinuum generation by the modulation instability," Opt. Comm. **244**, 181 (2005).

[12] A. Demircan and U. Bandelow, "Analysis of the interplay between soliton fission and modulation instability in supercontinuum generation," Appl. Phys. B **86**, 31 (2007).

[13] R. Driben, F. Mitschke, and N. Zhavoronkov, "Cascaded interactions between Raman induced solitons and dispersive waves in photonic crystal fibers at the advanced stage of supercontinuum generation," Opt. Exp. **18**, 25993 (2010).

[14] A. Demircan, Sh. Amiranashvili, C. Brée, C. Mahnke, F. Mitschke, and G. Steinmeyer, "Rogue events in the group velocity horizon," Sci. Rep. **2**, 850 (2012).

[15] T.G. Philbin, C. Kuklewicz, S. Robertson, S. Hill, F. Konig, and U. Leonhardt, "Fiber-Optical Analog of the Event Horizon," Science **319**, 1367 (2008).

[16] F. Belgiorno, S.L. Cacciatori, M. Clerici, V. Gorini, G. Ortenzi, L. Rizzi, E. Rubino, V.G. Sala, D. and Faccio, "Hawking Radiation from Ultrashort Laser Pulse Filaments," Phys. Rev. Lett. **105**, 203901 (2010).

[17] D. Faccio, "Laser pulse analogues of gravity and analogue Hawking radiation," Cont. Phys. **1**,1 (2012).

[18] R. Smith, "Reflection of short gravity waves on a non-uniform current," Math. Proc. Camb. Phil. Soc. **78**, 517 (1975).

[19] J.-Ch. Nardin, G. Rousseax, and P. Coullet, "Wave-Current Interaction as a Spatial Dynamical System: Analogies with Rainbow and Black Hole Physics," Phys. Rev. Lett. **102**, 124504 (2009).

[20] De Sterke, C. M., "Optical push broom," Opt. Lett. **17**, 914 (1992).

[21] Broderick, N. G. R., Taverner, D., Richardson, D. J., Ibsen, M. & Laming, R. I. "Optical Pulse Compression in Fiber Bragg Gratings," Phys. Rev. Lett. **79**, 4566 (1997).

[22] Rosanov, N., "Transformation of electromagnetic radiation at moving inhomogeneities of a medium," JETP Lett. **88**, 501–504 (2008).

[23] Rozanov, N., "Subluminal and superluminal parametric doppler effects in the case of light reflection from a moving smooth medium inhomogeneity," JETP **115**, 1063–7761 (2012).

[24] Lobanov, V. E. & Sukhorukov, A. P., "Total reflection, frequency, and velocity tuning in optical pulse collision in nonlinear dispersive media," Phys. Rev. A **82**, 033809 (2010).

[25] A. V. Yulin, D. V. Skryabin, and P. St. J. Russell, "Four-wave mixing of linear waves and solitons in fibers with higher-order dispersion," Opt. Lett. **29**, 2411 (2004).

[26] A. Demircan, Sh. Amiranashvili, and G. Steinmeyer, "Controlling light by light with an optical event horizon," Phys. Rev. Lett. **106**, 163901 (2011).

[27] P. V. Mamyshev, P. G. J. Wigley, J. Wilson, G. I. Stegeman, V. A. Semeonov, E. M. Dianov, and S. I. Miroshnichenko, "Adiabatic compression of Schrödinger solitons due to the combined perturbations of higher-order dispersion and delayed nonlinear response" Phys. Rev. Lett. **71**, 73–76 (2003).

[28] M. F. Saleh, W. Chang, P. Hölzer, A. Nazarkin, J. C. Travers, N. Y. Joly, P. St. J. Russell, and F. Biancalana, "Theory of Photoionization-Induced blueshift of Ultrashort Solitons in Gas-Filled Hollow-Core Photonic Crystal Fibers," Phys. Rev. Lett. **107**, 203902 (2011).

[29] Sh. Amiranashvili and A. Demircan, "Hamiltonian structure of propagation equations for ultrashort optical pulses," Phys. Rev. A. **82**, 013812 (2010).

[30] Sh. Amiranashvili and A. Demircan, "Ultrashort optical pulse propagation in terms of analytic signal," Adv. Opt. Tech. **2011**, 989515 (2011).

[31] V.E. Zakharov, V.S. Lvov, and G.E. Falkovich, *Kolmogorov Spectra of Turbulence I – Wave Turbulence*, Berlin, Springer (1992).

[32] J.M. Stone and J.C. Knight, "Visibly 'white' light generation in uniform photonic crystal fiber using a microchip laser," Opt. Express **16**, 2670 (2008).

[33] S. Batz, U. Peschel, "Diametrically driven self-accelerating pulses in a photonic crystal fiber," Phys. Rev. Lett. **110**, 193901 (2013).

[34] G. Genty, M. Lehtonen, and H. Ludvigsen, "Route to broadband blue-light generation in microstructured fibers," Opt. Lett. **30**, 756 (2005).

[35] S. Robertson and U. Leonhardt, "Frequency shifting at fiber-optical event horizons: The effect of Raman deceleration," Phys. Rev. A **81**, 063835 (2010).

[36] A.V. Yulin, R. Driben, B.A. Malomed, and D.V. Skryabin,"Soliton interaction mediated by cascaded four wave mixing with dispersive waves," Opt. Express **21**,14481 (2013).

[37] R. Driben, A.V. Yulin, A. Efimov, and B. A. Malomed, "Trapping of light in solitonic cavities and its role in the supercontinuum generation," Opt. Express **21**, 19091 (2013).

[38] A. Demircan, Sh. Amiranashvili, C. Brée, C. Mahnke, F. Mitschke, and G. Steinmeyer, "Rogue wave formation by accelerated solitons at an optical event horizon," Appl. Phys. B, DOI 10.1007/s00340-013-5609-9 (2013).

[39] F.M. Mitschke and L.F. Mollenauer,“Discovery of the soliton self-frequency shift,” Opt. Lett. **11**, 659 (1986).

[40] G. Genty, M. Surakka, J. Turunen, and A. T. Friberg, “Complete characterization of supercontinuum coherence,” J. Opt. Soc. Am. B **28**, 2301 (2011).